Supporting Information

Estimation of effective series resistance due to the hole transporter:

Devices were prepared as described in the previous section. The geometry of the in-plane two-point probe configuration was that of two long interdigitated electrodes with a channel length (direction of current flow) of 300 μm, a width of 6.53 cm, and a film thickness of 1 μm. The linear I-V curves obtained for these devices allowed us to calculate the conductivity by the standard method. It was approximated that 50% of the charge in the ss-DSSCs is generated within the first 500 nm of the devices due to the high extinction coefficient of the D102 dye used (see absorption spectra for 2 μm thick films of D102 sensitized TiO_2 films). We then took the mean distance for holes to be collected at the silver electrode to be equal to the remainder of the active area thickness (500 nm) plus the capping layer thickness (700 nm), to give 1.2 μm. The area through which the charge is transported is 0.09 cm^2 as defined by the solar cell mask aperture. We then used these dimensions together with the resistivities of spiro-OMeTAD at different doping concentrations to give the total resistance that could be expected through an ohmic series resistance to hole transport.

Ideal diode fit:

The current voltage curve was fitted numerically using the standard diode model, using least mean squares on the whole IV curve and fixing the open circuit voltage and short circuit current to match the experimental values.

Estimation of power losses through the devices due to series resistance:

For this analysis, the relevant J-V curves were modified to emulate the situation had there been 0 ohms of series resistance. The voltage point at each recorded current point was simply adjusted by adding $I \times R_s$ where I is the actual current (in amps) running through the 0.09 cm^2 active area of the solar cell and R_s is the series resistance as determined by the ideal diode fit. This corrected for the voltage drop to the built in series resistance in the cell. The theoretical (0 ohms R_s) maximum power point was then determined for each Li TFSI doping level and the difference with the real maximum power point was taken as a percentage of the maximum theoretical power point.

Estimation of possible conductivities of hole transporter:

To be more quantitative about the hole-transporter requirements, we can predict the conductivity values possible for hole-transporters with different hole mobilities at varying doping levels, assuming 100 % doping efficiency (see Supporting Information for details). When a hole-transporter such as Spiro-OMeTAD with hole mobility on the order of 2×10^{-4} cm^2 V^{-1} s^{-1} (an upper-end value based on time-of-flight measurements){Poplavskyy, 2003 #137} is used, a conductivity around 10^{-4} S cm^{-1} can be attained with just 1-4 mol % doping. The maximum conductivity attainable for this material, taking 10-20 mol % doping to be a practical limit and assuming a constant mobility, is then 1-2 $\times 10^{-3}$ S cm^{-1}. We note that the effective conductivities expected at these doping levels in a porous TiO_2 matrix should be lower by a factor of approximately three, and that the time-of-flight mobility should be an upper estimate, so that this really is an upper limit estimate. We can then conclude that a hole transporter with hole

mobility on the order of 10^{-3} cm^2 V^{-1} s^{-1} would allow for high conductivity values on the order of 10^{-3} S cm^{-1} upon doping below 5 mol %, which should allow for a more optimized system.

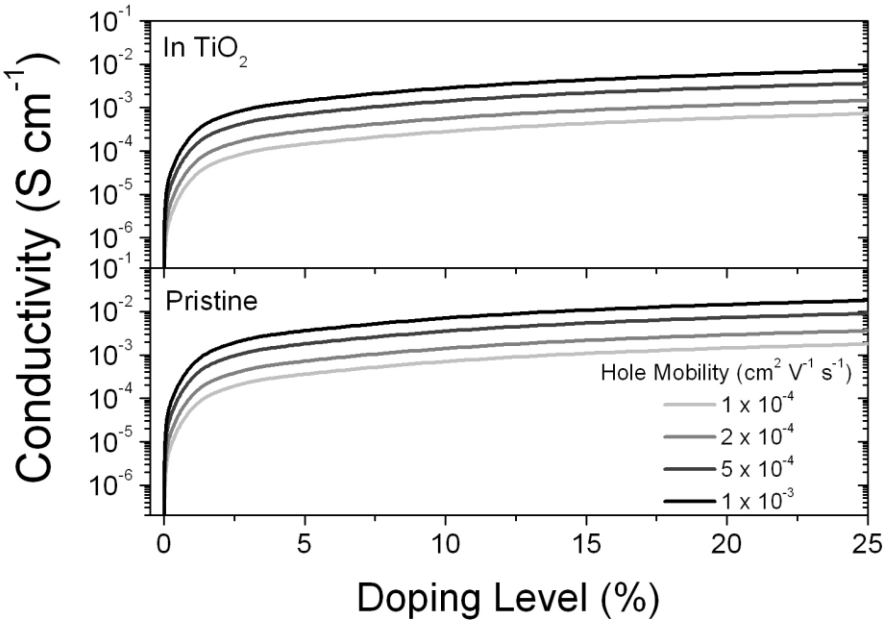

Figure 1S. Estimation of possible conductivities of hole transporter

The estimations were performed for the four different hole mobilities listed in the figure above by first calculating the molar density of spiro-OMeTAD in a pristine film assuming a volumetric density of 1 g cm^{-3} which is a value that has been confirmed in our laboratory. This yields a molar density of 4.9×10^{20} mol cm^{-3}. For a given doping percentage, the appropriate percentage of this molar density was taken to be equivalent to the hole density in the material. From this, it is straightforward to calculate a conductivity by the standard expression $\sigma = en\mu_h$ where e is the unit of elementary charge,

n is the hole density calculated as described above, and μ_h is the hole mobility. To then estimate the effective conductivity as it would be measured in a mesoporous film of TiO_2, a porosity of 0.5 % was assumed for a system having undergone $TiCl_4$ treatment and dye sensitization, with an upper-end value for the pore filling fraction of hole conductor into the pores of 80 %. This allows us to calculate an adjusted spiro-OMeTAD molar density of 2.0×10^{20} mol cm^{-3} inside the mesoporous film, and calculate the appropriate conductivity values.

Metal-semiconductor contact resistance:

Electrical impedance spectroscopy was used to confirm that the conductivity of doped and undoped spiro-OMeTAD thin-films measured using two contact electrodes in a planar configuration was not dominated by the contact resistance. The Nyquist plots taken at frequencies from 10 Hz–1 MHz of the impedance spectra for an undoped sample and a sample doped with Li-TFSI are shown in Figure 4S.

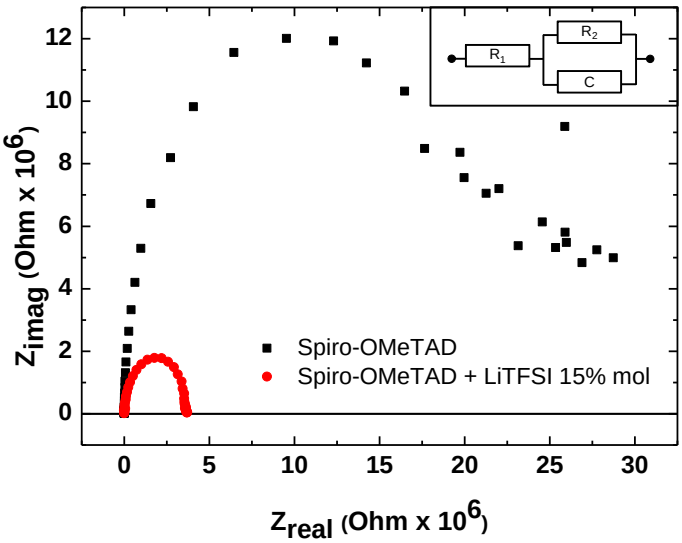

Figure 2S: Nyquist plots obtained from electrical impedance spectroscopy of spiro-OMeTAD with and without doping with LiTFSI. Inset: equivalent circuit used for extracting the device parameters.

The equivalent circuit used to model the device is shown in the inset to Figure 2S where R_2 represents the resistance of Spiro-OMeTAD, C represents the sample capacitance due to the dielectric response of Spiro-OMeTAD, and R_1 represents the series resistance. The parameters extracted from the plots shown in Figure 4S are summarised in Table 1S.

TABLE 1S: Summary of equiavalent circuit parameters extracted from electrical impedance spectroscopy measurements.

Sample	R_1 (kΩ)	R_2 (MΩ)	C (pF)
Spiro-OMeTAD	1.99	25.1	164
Spiro-OMeTAD + Li-TFSI 15 % mol	2.64	3.62	150

In the equivalent circuit, the series resistance includes the contact resistance which we know to be ohmic from the straight line observed in the two-probe current-voltage characteristics. We find that in both systems R_1 does not significantly change despite the significant change in R_2. This suggests that the two-probe measurements are dominated by the high resistance of the conductive channel and not the contacts. The values of R_2 are in close agreement with the two-probe conductivity measurements.

Solid state ^{7}Li NMR:

^{7}Li solid state NMR spectra were recorded at 155.45 MHz on a Bruker Avance II spectrometer equipped with a 4 mm MAS probe. A $\pi/2$ pulse width of 4.5 μs was used, with a relaxation delay of 120 s and a spinning speed of 8-10 kHz. Chemical shifts are referenced to external LiCl (aq) 1 M.

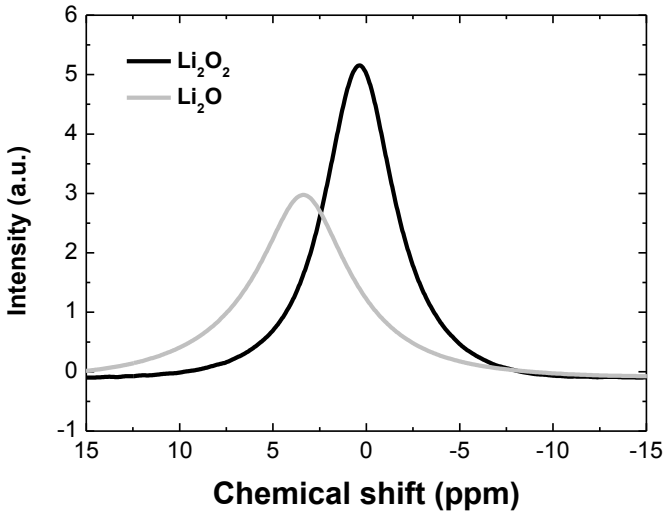

Figure 3S. Li_2O_2 and Li_2O solid state ^{7}Li NMR

Ground state dye absorption:

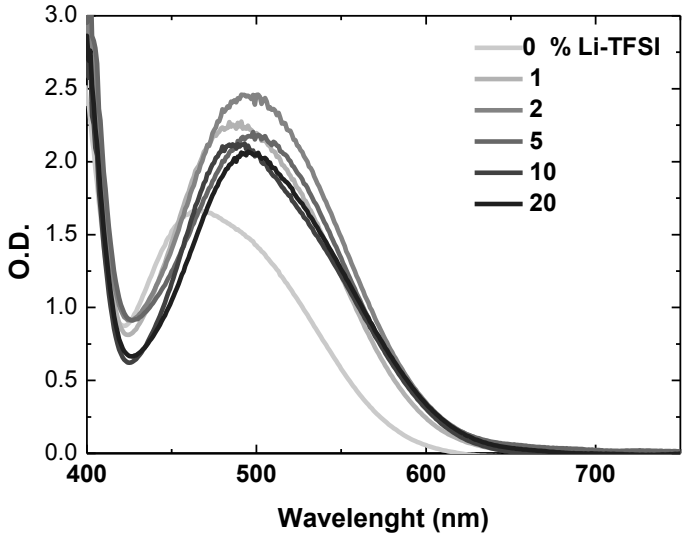

Figure 4S. Absorbance spectra of a 2 μm D102 sensitized TiO_2 substrates taken in an integrating sphere. *t*bp was kept at the constant concentration specified in the main text.

Spiro-OMeTAD on SiO_2 conductivity in dry O_2:

We prepare conductivity devices similar to those described before, but using mesoporous SiO_2 instead of TiO_2 and testing them in pure oxygen instead of air.

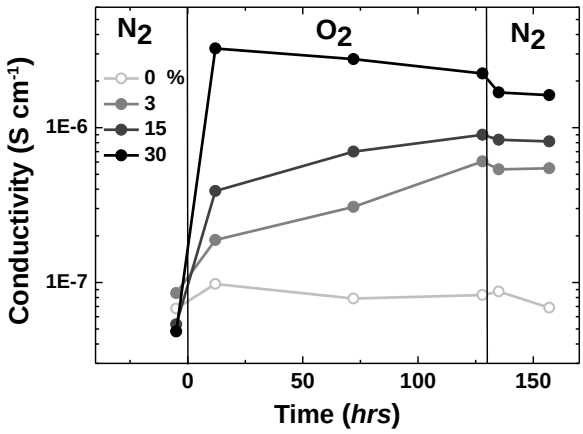

Figure 5S. Spiro-OMeTAD conductivity as function of the Li-TFSI content (mol %) for film on SiO_2. The samples were stored and measured in dark.

Explanation of Figure 2b:

We note that there is a 2-fold decrease in conductivity of the un-doped spiro-OMeTAD upon exposure to air. To explain this, we note that TiO_2 nanoparticles used in our devices have been shown to contain reduced Ti^{3+} cations at the surface due to the presence of oxygen vacancies (J. Phys. Chem. C 2010, 114, 16937–16945). Oxygen has been reported to adsorb to these sites (*J. Phys. Chem. B*, 1999, 103 (25),5328–5337) forming O_2^-, a powerful reducing agent. We postulate that these may interact with holes in the spiro-OMeTAD to reduce the overall mobility by a trapping / detrapping mechanism. A quantitative analysis of this phenomenon is beyond the scope of this work, but the data presented in Figure 5S shows the influence of oxygen exposure on films not containing TiO_2. In this case, the conductivity of the spiro-OMeTAD does not appear to be higher in nitrogen atmosphere, which fits with the explanation proposed above.

References:

(1) Docampo, P.; Guldin, S.; Stefik, M.; Tiwana, P.; Orilall, M. C.; Hüttner, S.; Sai, H.; Wiesner, U.; Steiner, U.; Snaith, H. J. *Advanced Functional Materials* 2010, *20*, 1787.

(2) O'Regan, B. C.; Lenzmann, F. *The Journal of Physical Chemistry B* 2004, *108*, 4342.

(3) Bisquert, J.; Zaban, A.; Greenshtein, M.; Mora-Seró, I. *Journal of the American Chemical Society* 2004, *126*, 13550.

(4) Strunk, J.; Vining, W. C.; Bell, A. T. *The Journal of Physical Chemistry C* 2010, 114, 16937.

(5) Henderson, M. A.; Epling, W. S.; Perkins, C. L.; Peden, C. H. F.; Diebold, U. *The Journal of Physical Chemistry B* 1999, 103, 5328.